Trapped Aqueous Films Lubricate Highly Hydrophobic Surfaces

Trapped Aqueous Films Lubricate Highly-Hydrophobic Surfaces.

Irit Rosenhek-Goldian‡, Nir Kampf‡, and Jacob Klein*

Dept. of Materials and Interfaces, Weizmann Institute of Science, Rehovot 76100, Israel

‡ These authors contributed equally

* Jacob.klein@weizmann.ac.il

Abstract

Friction at hydrophobic surfaces in aqueous media is ubiquitous (*e.g.* prosthetic implants, contact lenses, microfluidic devices, biological tissue), but is not well understood. Here we measure directly, using a surface force balance, both normal stresses and sliding friction in an aqueous environment between a hydrophilic surface (single-crystal mica) and the stable, molecularly-smooth, highly-hydrophobic surface of a spin-cast fluoropolymer film. Normal-force vs. surface-separation profiles indicate a high negative charge density at the water-immersed fluoropolymer surface, consistent with previous studies. Sliding of the compressed surfaces under water or in physiological-level salt solution (0.1M NaCl) reveals strikingly low boundary friction (friction coefficient $\mu \approx 0.003 - 0.009$) up to contact pressures of at least 50 atm. This is attributed largely to hydrated counterions (protons and Na^+ ions respectively) trapped in thin interfacial films between the compressed, sliding surfaces. Our results reveal how frictional dissipation may occur at hydrophobic surfaces in water, and how modification of such surfaces may suppress this dissipation.

keywords

hydrophobic surfaces; hydration lubrication; hydrophobic hydration; aqueous thin-films; hydrophobic lubrication.

Friction at hydrophobic surfaces is ubiquitous, from underwater cables to biomedical devices and biological tissues.[1-10] While the properties of hydrophobic surfaces in contact with water, including their hydrophobicity, their interfacial energies and their propensity for adsorption, as well as their surface interactions, have been studied extensively,[11-21] much less is known about the frictional dissipation processes at such surfaces. Such friction may result from multiple dissipation pathways, including plastic and viscoelastic deformations, the breakage of strong bonds in creation of wear debris, or intrinsic boundary dissipation arising from short-ranged interactions during sliding.[22,23] We are particularly interested in the sliding of a hydrophilic surface past a hydrophobic one, as this sheds strong light on the relevant interfacial dissipation mechanisms.

Forces between surfaces play an important role in frictional dissipation as they slide past each other. In contrast to the many studies of symmetric (hydrophobic vs. hydrophobic[11]) interactions across aqueous media, there are relatively few investigations of a stable hydrophobic surface interacting with a hydrophilic one.[24-31] In most of these studies the hydrophilic surface (usually mica or silica) is negatively charged under water, and force vs. surface-separation profiles in water with pH $\gtrsim$ 5.5 – the usual ambient or biological conditions - show a long-ranged repulsion, becoming shorter ranged on adding salt.[24,25,29,30] This behavior is consistent with a negative charge on the opposing hydrophobic surface, as well as with ζ-potential measurements on various hydrophobic solids in aqueous media,[24,25,29,30,32-34] including in particular AF surfaces.[34,35] In the few studies where sliding friction between hydrophobic and hydrophilic surfaces was measured,[5,36,37] using tipped or colloid-

tipped AFM, rather high friction coefficients were observed (coefficient of sliding friction $\mu \gtrsim 0.1$), though interpretation of the results may be complicated by contact adhesion, indeterminate contact separation and roughness of the probe.

In the present study, using a surface force balance (SFB), we examine normal forces and, in particular, the sliding friction between a smooth hydrophilic surface – a crystallographically-smooth sheet of cleaved mica - and an opposing, highly hydrophobic, smooth fluoropolymer film. The rigidity, impermeability, smoothness and stability of the solid fluoropolymer surface are necessary for enabling a large range of pressures and for ensuring that sliding friction between the surfaces is determined by dissipation at the hydrophilic/hydrophobic interface alone. Interactions are measured in water (no added salt) as well as in high concentration salt solution. The normal force profiles reveal both the nature of the interactions as well as the sign and magnitude of the surface charges. Shear forces, measured directly as the surfaces slide at different loads and velocities at a known separation (to ±0.3 nm), may reveal the mechanism of the frictional dissipation processes.

Results and Discussion

Molecularly smooth, stable, highly hydrophobic surfaces were created by spin-casting an amorphous fluoropolymer film (henceforth AF) onto a freshly-cleaved, single-crystal mica sheet, which was glued to a plano-cylindrical lens for mounting into the SFB (Methods). Their characteristics are given in figure 1.

Normal forces $F_n(D)$ and lateral (friction) forces F_s between a curved hydrophilic mica surface and the curved hydrophobic AF surface, in a crossed-

cylinder conformation (mean radius of curvature R, closest distance D apart) were measured in an SFB[38] (Methods and inset to fig. 2). Importantly for estimating (below) the confined interfacial film, we measured the AF film thickness in adhesive air contact with the mica ($D = D_{\text{air-contact}}$), then immersed the surfaces in water and, at the same contact point, measured the limiting film ('hard wall') thickness at the highest loads, $D = D_{\text{hard-wall}}$. Within our spatial resolution in D (±0.3 nm) these two values were the same, $D_{\text{air-contact}} = D_{\text{hard-wall}}$. Force profiles in all cases were reversible and reproducible, within a scatter attributable to thermal drift; to variations in the effective salt concentration and surface potential on both mica and AF surfaces (the latter arising from small pH differences[34]); to possible non-uniformity of the charge distribution on the AF surface; and (for F_s) to small differences in local roughness of the AF surface (fig. 1A and below). It is worth remarking, as seen in fig. 2A, that scatter of data at a given contact point was significantly smaller than at different contact point or different experiments, supporting the attribution above. Maximal mean pressures P across the flattened contact area between the surfaces (Methods) were around 5 MPa (ca. 50 atm). We note that when the mica and AF-coated mica were in *air contact*, prior to adding water, the friction force between them was larger than the maximal shear force that could be applied through bending the shear springs *via* the sectored PZT, corresponding to a friction coefficient in air contact $\mu_{\text{air-contact}} > 0.05$.

Figure 2A shows $F_n(D)/R$ profiles in purified water with no added salt (see Methods; henceforth: water). For D $\gtrsim$ 5 nm the monotonic repulsion between the surfaces is well described by the non-linear Poisson-Boltzmann equation (PB) augmented by the appropriate van der Waals (vdW) attraction,[39] (PB + vdW), indicating that it is due to the osmotic pressure of counterions trapped between two

same-sign charged surfaces. As mica under water is negatively charged,[40,41] fig. 2A shows unambiguously that the hydrophobic AF surface is also negatively charged under water (since an uncharged AF surface, blue curve in fig. 2A, would strongly under-predict the repulsion), though our measurements do not reveal the origin of the charge (see Supplementary Information (SI) section 5). These results showing a negatively-charged AF surface are in line with earlier hydrophilic-hydrophobic surface force studies (noted above[24,25,29,30]), and with the ζ-potential measurements on hydrophobic solids, including AF surfaces[24,25,29,30,32-35] and oil-water interfaces (*e.g.*[42]). The $F_n(D)/R$ data in fig. 2A is well fitted by a value of σ^{AF} indicated by earlier studies of fluoropolymer-water surface potentials[34] (SI section 4), as seen by the black curve in fig. 2A. At a separation D < 1-2 nm, clear deviations from the (PB + vdW) fit are observed. In particular, a sharp rise in $F_n(D)/R$ is measured rather than the predicted approach into vdW adhesive contact across water,[39-41] and no net attraction between the surfaces on separation even following the strongest compressions. This is attributed to repulsion due to hydrated counter-ions trapped between the negatively-charged surfaces;[40,43] in purified water with no added salt (as in fig. 2A) these are predominantly hydrated protons (hydronium ions). Such hydronium counter-ions are known to condense into (and neutralize) the negatively-charged lattice sites on the mica surface[40,41] at $F_n(D)/R \gtrsim 1$ mN/m. Their persistent presence in the gap at much higher $F_n(D)/R$ values (fig. 2A) is thus attributed to the high negative charge density on the AF surface alone. This is because the overall concentration of these trapped ions is much higher than can condense into the mica lattice (as illustrated schematically in the inset to fig. 3b).

On increasing the salt concentration in the water to 0.1 M NaCl, the range of the repulsive forces is greatly reduced relative to that measured across pure water, as expected for double-layer electrostatic repulsion,[39] as seen in figure 2B (where for D $\gtrsim$ 5 nm the Debye screening length is ca. 1 nm). As in the water, measurements in the salt solution were (within the scatter) reversible and reproducible on subsequent approaches. The increasingly strong repulsion between the surfaces at $D < 2 – 3$ nm, together with the absence of any adhesion on separation, again indicates hydration repulsion, which at the high salt concentration is predominantly due to trapped, hydrated Na^+ ions.[40,43] Since, unlike hydrated protons, the hydrated Na^+ ions do not condense into the mica surface even at high *P,*[44] one expects both the hydrophobic AF surface and the mica surface to retain a net (negative) charge up to the highest compressions (ca. 5 MPa) in our study.

Friction forces F_s between the mica and AF surfaces as they were made to slide past each other at different compressions (different loads F_n) in aqueous media are shown as typical time traces $F_s(t)$ in fig. 3A, and summarized in fig. 3B. As seen in fig. 3B, F_s is found to increase linearly with F_n, corresponding to a sliding friction coefficient $\mu = (F_s/F_n)$ in the range $\mu = 0.003$-0.009 up to the maximal pressures applied ($P \approx 50$ atm). This very low friction up to high pressures between a hydrophilic surface and a highly hydrophobic surface is the main, and unexpected, finding of this study.

Finally, in fig. 4 we show the variation of the friction force F_s with sliding velocity v_s over several orders of magnitude in v_s. Such variation, as discussed further below, provides insight concerning the energy dissipation mechanisms as the contacting surfaces slide past each other.[23,45]

What is the origin of the remarkably low frictional dissipation as the highly-hydrophilic mica and highly-hydrophobic AF surfaces slide past each other? We recall the long-known, low friction (and high wear) associated with sliding past poly(tetrafluoroethylene) (PTFE) surfaces in macroscopic tribology, which is due to transfer of coherent PTFE films between the sliding surfaces and the consequent easy shear between chains.[46] The resulting sliding friction coefficients for rubbing past such PTFE surfaces are in the range 0.05 – 0.2, at least an order of magnitude higher than measured in our study. More directly, our reproducible and reversible normal force profiles show explicitly that no transfer of the AF occurs between the bare mica and the AF-coated mica surfaces, as such transfer would lead to a long-ranged steric repulsion on second approach at a given contact point following shear. This is because any transfer of material from one surface to the other would result in a disordered accumulation of polymer molecules on the opposing surface, and hence a long-ranged steric repulsion.[47] Likewise, no wear occurs between the surfaces on shear and sliding, as that would be immediately seen in the change of absolute separation between the surfaces when they are compressed to contact. In practice the second and subsequent 'hard-wall' separations at a given contact are identical to the first profile (within the scatter of ca. 0.5 nm), despite the extensive shear and sliding between the surfaces on each approach. Moreover, any steric repulsion arising from film transfer would be independent of salt concentration, since the configuration of transferred, neutral fluoropolymer chains, if there were any, would not depend on the salt concentration. At the same time, the range of repulsion of the normal force profiles in water with no added salt, and in 0.1M salt solution, depends strongly on the salt concentration and scales as the Debye screening length, as expected between

smooth charged surfaces. These observations, together with the order of magnitude reduction in friction from air contact to its value μ under water ($\mu_{air\text{-}contact} > 0.05$ to $\mu \approx 0.005$) clearly show that the 'film-transfer' mechanism responsible for PTFE friction in air does not apply in our experiments. In this connection we also note that in very recent experiments[48] comparably low friction was measured also between a hydrophilic (mica) and a different hydrophobic (octadecanethiol-coated gold) surface under water and salt solutions, confirming that the effect we observe is not unique to hydrophobic fluoropolymer-coated surfaces.

We consider also the possibility of nanobubble formation on our AF coated surfaces. While there is no evidence that nanobubbles reduce friction between sliding surfaces, we have also not detected their formation on our hydrophobic AF surface, as our AFM micrographs (*e.g.* fig. 1A) clearly reveal a smooth surface free of the structure characteristic of nanobubbles.[49-51] In addition, the interaction between a hydrophilic solid surface and an air bubble has been directly measured.[26] This shows marked *attraction* below separations of ca. 40 nm between the air-bubble-surface and the hydrophilic solid surface, attributed at least in part to electrostatic effects. This is very different to the monotonic *repulsion* between the bare hydrophilic mica and the hydrophobic AF-coated mica which we measure (fig. 2A), further supporting the conclusion that nanobubbles are absent. Furthermore, if any nanobubbles were present on the AF surface, and were to bridge the gap to the mica surface (drying it), then on collapse of such bubbles as the surfaces approach, water-free contact between the bare mica and the AF layer would be formed. This would result in a consequent high friction, since $\mu_{air\text{-}contact} > 0.05$, which is not observed. In contrast, if nanobubbles are present but do not bridge the gap, and the mica surface remains wetted as it approaches the hydrophobic surface, then water remains trapped between the mica

and AF surface when they come into contact at high pressures as the nanobubbles collapse (D < ca. 0.5 nm). This trapping of water between the surfaces is precisely the scenario we propose, and implies that nanobubbles would not contribute to the reduction in friction even if they were present (which is highly unlikely for the reasons just noted). These observations taken together strongly indicate that nanobubbles are not present at our hydrophobic surface, and that even if they are they do not contribute to the strong lubrication we measure.

Since the sliding friction coefficient decreases abruptly from its air value ($\mu_{air\text{-}contact} > 0.05$), once water is added, by an order of magnitude or more (to $\mu \approx 0.005$), the reduction in the friction must arise from the presence of water between the surfaces. Since free water would be squeezed out from between the smooth surfaces, as observed between neutral mica surfaces,[52] we attribute the low friction rather to lubrication mediated by the hydration shells surrounding counterions trapped between the surfaces (so-called hydration lubrication.[43,45] Such hydration repulsion was also predicted in ref.[53]). It is also possible that the mobility of charges at the hydrophobic AF surface contributes to this lubrication,[54] or that some slip of the trapped hydration water at the AF surface, as seen with other hydrophobic surfaces,[55] reduces the frictional dissipation. In all cases, however, the essential feature is the trapping of the hydrated ions between the charged surfaces. In water (fig. 3A, green symbols) hydrated (positively-charged) hydronium counter-ions are trapped between the compressed surfaces due to the negatively-charged AF, as illustrated in the top cartoon in fig. 3A. It is appropriate to note that the depiction of a uniform charge density on the AF surface in these cartoons (fig. 3) is purely for illustration purposes and cannot be deduced from the data of fig. 2. Indeed, some of the scatter in the $F_n(D)/R$ profiles may be attributable to locally non-uniform (negative) charge

distribution on the AF surface. As the surfaces slide past each other, there are two different scenarios which may account for the low friction. In the case that the negative charges at the AF surface are immobile or have low lateral mobility, dissipation will occur through viscous losses arising from shear of the tenaciously-attached hydration shells[56] surrounding the hydronium ions localized at these surface charges. This mechanism is known to lead to very low friction ($\mu < 10^{-3}$) up to high pressures.[43, 45] For the case where the negative charges on the AF surface are laterally very mobile, they may themselves, with their localized counter-ions, respond to shear by sliding across the AF substrate.[54] Clearly, a combination of these two different modes would also lead to low frictional dissipation. Additionally, slip of the sheared, trapped hydration water may occur at the highly hydrophobic surface[54] (where stick boundary conditions relevant to hydrophilic surfaces may not apply[55]), further reducing the frictional dissipation.

The absolute thickness of the trapped hydrated counterion layer is difficult to measure directly because the AF layers vary slightly in thickness across their area. However, the observation that at a given contact point the thickness of the AF layer is identical (within our resolution of ± 0.3 nm) both in air ($D = D_{\text{air-contact}}$) and under strong compression in water ($D = D_{\text{hard-wall}}$) provides an estimate of its thickness. This is because under water the hydrocarbon-based layer (of thickness ~0.5 nm), which is known to adsorb onto mica from ambient atmosphere, is dissolved away,[57] so that this observation – $D_{\text{air-contact}} = D_{\text{hard-wall}}$ – implies a thickness of the trapped hydronium ion layer which is itself around 0.5 nm. In other words, the zero of contact between the AF layer and the mica in air is identical to its value in water, implying that the ca. 0.5 nm thick carbonaceous layer has been replaced by a similarly-thick aqueous layer. This thickness is consistent with the diameter of hydrated protons, which is ca. 0.55

nm.[56,58] It is also comparable to the thickness of the trapped layer of hydrated Na^+ counterions between two bare mica surfaces compressed to similar contact pressures across 0.1M salt solution.[45,59]

When water is replaced by 0.1M NaCl solution the mean frictional dissipation remains very low (black symbols, fig. 3B). This is attributed, as for the water case, to lubrication by trapped hydrated counter-ions, which for the case of the high salt solution are predominantly Na^+ ions. The trapped counter-ion concentration in this case is likely higher than in the pure water case, since, as noted, hydrated Na^+ ions do not condense into the mica surface, and so must compensate for the charges on both surfaces. This higher concentration of trapped hydrated metal counter-ions, as well as their larger size,[56,58] may underlie the (possibly) improved lubrication in the salt solution (black vs green data in fig. 3A). In addition, as noted for the water case, high lateral mobility of the negative charge[54] as well as slip of water on the AF surface[55] may also contribute to reduction of friction.

Further insight is provided by the dependence of the friction force F_s on the applied sliding velocity v_s, as shown in figure 4 for 3 different loads (and different contact points). The marked logarithmic variation $(F_s - F_{s,0}) = (\text{constant}) + (\text{constant})\ln(\underline{v}_s)$ at each load over several exponential orders (where $F_{s,0}$ is a small systematic effect, Methods), is a clear signature of rate activated sliding,[44,45,60] where the basic sliding step associated with energy dissipation requires the overcoming of an energy barrier (Methods). In the present case, we attribute this barrier to localized shear and deformation of AF asperities in adhesive vdW contact with the mica surface. Such asperity contact, arising from the small but finite roughness of the surface (fig. 1A), provides an additional frictional dissipation pathway to those described above. However, such contacts are expected to constitute only a small

fraction of the overall contact area, while the trapped counter-ions and their associated lubricating hydration layers reside over most of the interfacial gap and so dominate the frictional dissipation. This scenario accounts for several features: The absence of net adhesion as the surfaces separate (Fig. 2) arises because the hydration repulsion in the trapped interfacial layer exceeds any AF-asperity/mica adhesion; the 'stick' of the surfaces prior to commencing sliding (fig. 3A) corresponds to the initial yield of the adhering AF asperities; and the relatively large scatter in F_s (fig. 3B) may arise because the characteristic lateral length scale of local roughness variation, of ca. 10 μm (fig. 1A), is comparable with the lateral dimensions of the AF-mica contact area, so that different contact points may experience different extents of asperity contact. It is appropriate to note – though it is beyond the scope of the present study - that approach to contact between two hydrophobic surfaces in water (as opposed to hydrophobic/hydrophilic as here) leads to cavitation or nanobubble formation between them (see SI section 6), so that the AF/water interface disappears and the concept of interfacially-trapped hydrated ions between them, as discussed in the present study, no longer apply.

Conclusions

We have shown that friction in water between a hydrophobic and a hydrophilic layer may be extremely low up to physiologically-high pressures (at least 50 atm), attributed largely to lubrication by nanometrically-thin interfacial layers consisting of hydrated counterions trapped by surface charges. These results may be relevant for understanding biological lubrication processes, where hydrophobic and hydrophilic biological tissues frequently interact. They may also have implications for

design of hydrophobic surfaces that minimize sliding friction, by optimizing the conditions – for example, extent of surface charge under water – that promote the trapping of such thin hydration-water films.

Materials and methods

Materials: Muscovite mica was used as the interacting model substrate surfaces (high grade (V1), S&J Trading Inc., NY). For SFB experiments, mica sheets were prepared as described previously.[57] NaCl was purchased from Merck (99.999% purity). Water was purified using a NanoPure Diamond system, Barnstead, USA, with resistivity ≥ 18.2 MΩ·cm and total organic carbon <1 ppb, and pH in the range 6±0.2). Teflon Amorphous Fluoropolymer - AF 1600 (AF) was purchased from DuPont, as a 6% solution of Teflon AF 1600 (AF) dissolved in a perfluorinated solvent Fluorinert™ Electronic Liquid FC-40 supplied by 3M, and used as received. Structural details of these fluoro-compounds are given in SI section 1.

AF film preparation: All preparations and experiments were at room temperature (25±1 ºC). A droplet of Teflon AF 1600 (AF) solution (6% in FC-40) was spin coated on bare mica surface for 90 sec at 6000rpm in a dust-free environment. For contact angle measurements the surfaces were prepared using this same procedure, but on a 1x2 cm freshly cleaved flat mica surface. In all SFB experiments the dry AF coated mica lenses were washed under a stream of pure water for a few seconds, and immediately mounted in the SFB. The AF films, of thickness ca. 400 nm (uniform to 1% over the film area), adhered stably to the underlying mica surface following 5 days immersion in water, and could withstand, without damage or detachment, the highest compressive or frictional stress applied to the surfaces in our experiments.

Atomic force microscopy (AFM) imaging: Imaging and surface topography was carried out using a MFP-3D SA (AFM) instrument (Oxford Instruments Company, Asylum Research, Santa Barbara, CA). To resemble SFB measurements conditions, AF-coated mica surface was scanned in tapping mode under water using a silicon nitride V-shaped 115μm long cantilever with a nominal spring constant of 0.35 N/m and a pyramidal silicon tip (SNL, Bruker).

SFB measurements: The experimental procedures used to measure the absolute separation D and the normal and shear forces between mica surfaces using a surface force balance (SFB), shown schematically in the inset to fig. 2, have been described in detail elsewhere,[38] including determination of the small systematic signal $F_{s,0}$, fig. 4 (SI sections 2 and 3). The zero of separation in force profile measurements (D = 0, fig. 2) was set to its value at the highest loads measured at each contact point, avoiding differences arising from the slight AF film-thickness variation. Normal and friction force profiles (figs. 2 and 3) are based on measurements from 4 independent experiments (different pairs of mica and AF surfaces) and different contact points within each experiment. Friction force F_s vs. F_n results, fig. 3B, are based on shear traces taken over a total of 12 different approach (and in several cases also separation) profiles from the 4 independent experiments.

Evaluation of mean pressures *P*: We used the Hertzian contact mechanics relation[39] for the radius a of a flattened region between a sphere radius (radius R) compressed with load F_n on a non-adhering flat (equivalent to our geometry of crossed cylinders with mean radius of curvature R), $a = (F_n R/K)^{1/3}$, where K is an effective modulus. The contact area is then $\mathcal{A} = \pi a^2$. K was determined separately from several experiments where a was measured as a function of F_n, and had a mean value K =

(5±2) x 10^9 N/m^2. This value was used to evaluate the mean contact pressures $P = F_n/\mathcal{A}$; we estimate an uncertainty of ±25% in the absolute value of P arising from uncertainties in K and in R.

Evaluating $F_n(D)/R$ *via* the Poisson–Boltzmann (PB) equation: The PB equation relates the potential to the distribution of the counter ions near a charged surface.[39,61] For the 1-D configuration relevant to our experiments and a 1:1 electrolyte:

$$\nabla^2\psi = (2ec_b/\varepsilon\varepsilon_0)\sinh(e\psi/k_BT) \qquad (1)$$

where $\psi(x)$ is the potential at distance x from the surface, e the electronic charge, and ε and ε_0 the dielectric constant (of water in this case) and permittivity of free space respectively, and c_b is the concentration of ions in the bulk solution. This may be solved numerically for the osmotic pressure $\Pi(D)$ between two charged surfaces, in our case with fixed (unequal) charge boundary conditions,[61] which is integrated to yield the interaction energy/area between flat parallel plates, $W = \int_{\infty}^{D} \Pi(D')dD'$. The force $F_{e\text{-}s}(D)$ between curved surfaces (mean radius of curvature R) a closest distance D apart obeying the same electrostatic double-layer interaction, is given in the Derjaguin approximation ($D \ll R$) by $F_{e\text{-}s}/R = 2\pi W$. This is augmented by the van der Waals attraction $F_{vdW}/R = -H/(6D^2)$, where H is the Hamaker constant, to yield $F_n(D)/R = 2\pi W - H/(6D^2)$. We use H = 1.18 x 10^{-20} J, which is the average of the H values for mica-water-mica and AF-water-AF.[62] The blue curve in fig. 2A was calculated as above using constant charge boundary conditions for a characteristic mica negative charge density[63] $\sigma^{mica} = -e/(66.5nm^2)$, with $\sigma^{AF} = 0$ and a 1:1 electrolyte concentration c_b = 8 x10^{-5}M (the presence of ions in water with no added

salt arises from dissolved ambient CO_2 and leached ions from glassware), while the black curve was calculated using the same parameters save that $\sigma^{AF} = -e/(9\ nm^2)$.

Rate activated sliding: When the basic step associated with frictional dissipation between two sliding surfaces requires the overcoming of an energy barrier, the sliding may proceed *via* Eyring-like rate activated processes.[60] We apply a detailed analysis of the resulting friction F_s, as given in refs.[44,45] for sliding of highly compressed surfaces, where in our experiments the barrier ΔE arises from localized shear and deformation of AF asperities in adhesive vdW contact with the mica. For a given load at varying sliding velocities v_s, one finds[44]

$$F_s = (\mathcal{A}/\Omega)\Delta E + (\mathcal{A}k_BT/\Omega)\ln(v_s) \qquad (2)$$

where $\mathcal{A}$ is the contact area at the given load and Ω is a stress activated volume. This is the form of the $F_s(v_s)$ variation seen in fig. 4.

Acknowledgements

We thank the Caesarea Foundation, the European Research Council (Advanced Grant CartiLube), the Petroleum Research Fund administered by the American Chemical Society (Grant 55089-ND10), the McCutchen Foundation and the Israel Science Foundation for their support of this work. We thank Sylvie Roke, Ran Tivony and Geraldine Richmond for helpful discussions, and JK thanks Richard Saykally for useful correspondence. This work was made possible in part by the historic generosity of the Harold Perlman family.

Figures

A

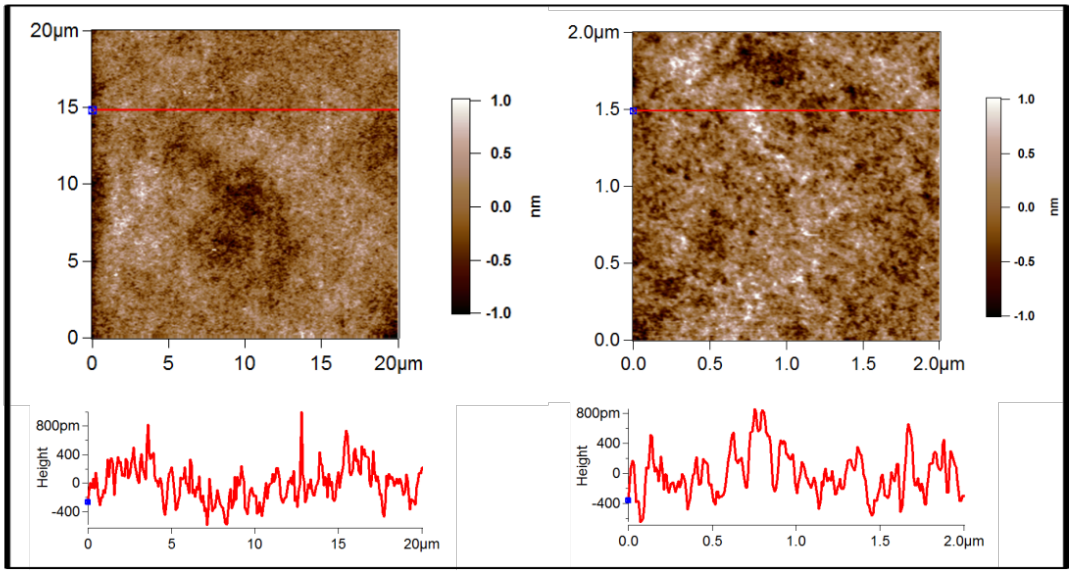

B

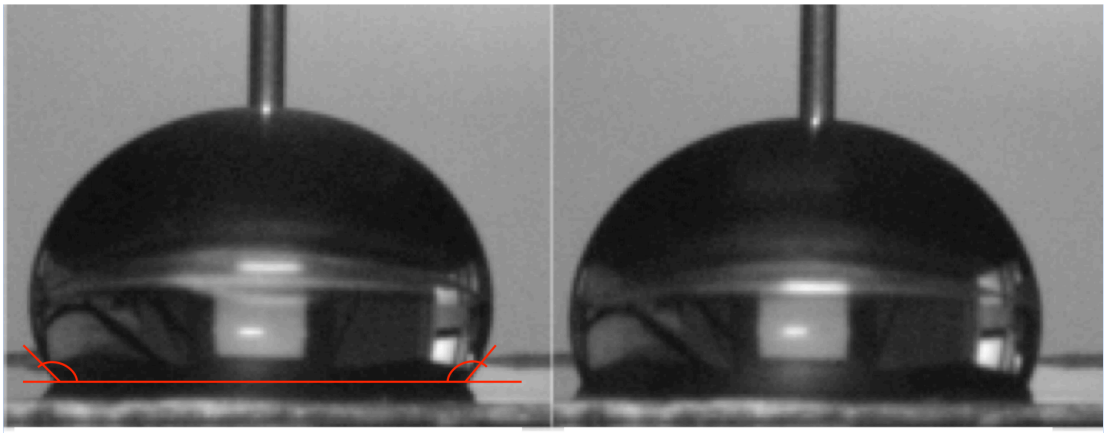

Figure 1: Characterizing the AF surfaces. (A): AFM images, at two different scan areas, of AF film spin cast on mica scanned under water; RMS surface roughness over the 20 x 20 µm scan (left image) is 0.27 nm; average RMS surface roughness taken over several similar films is 0.37 ±0.04 nm. (B): typical examples of water droplets advancing (left) and receding (right) on AF spin cast on mica. Values of contact

angles shown, measured using a First Ten Angstroms goniometer, model FTA200, are the mean of several measurements and were unchanged following 5 days immersion in water.

A

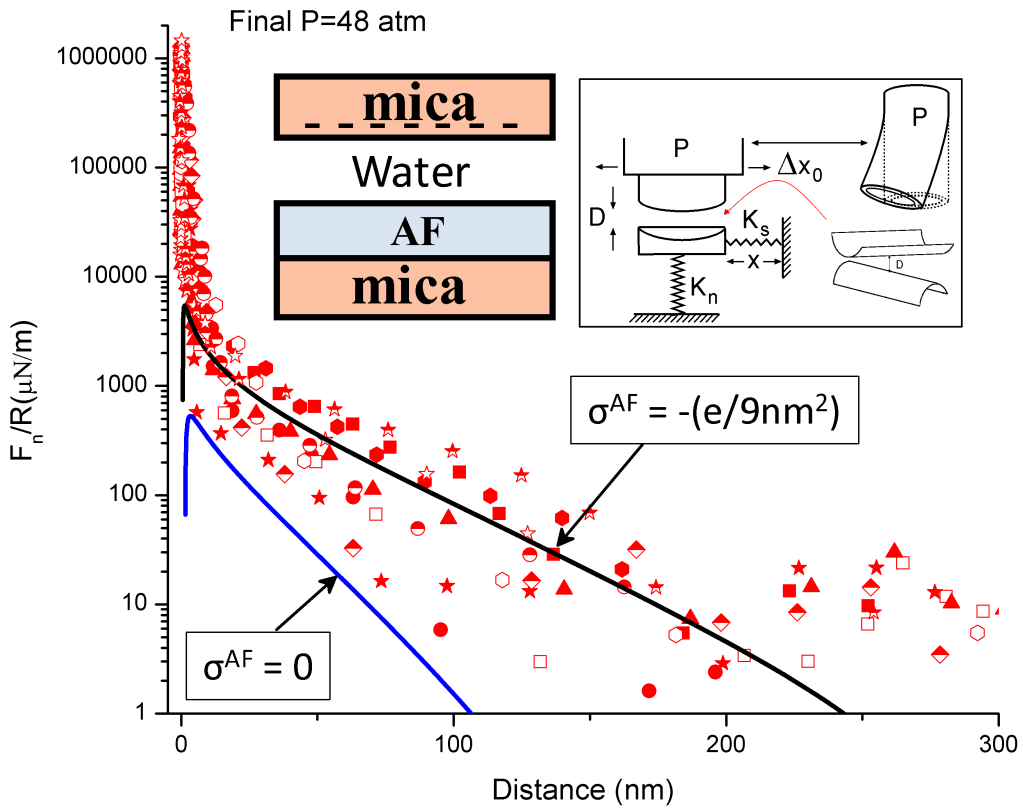

B

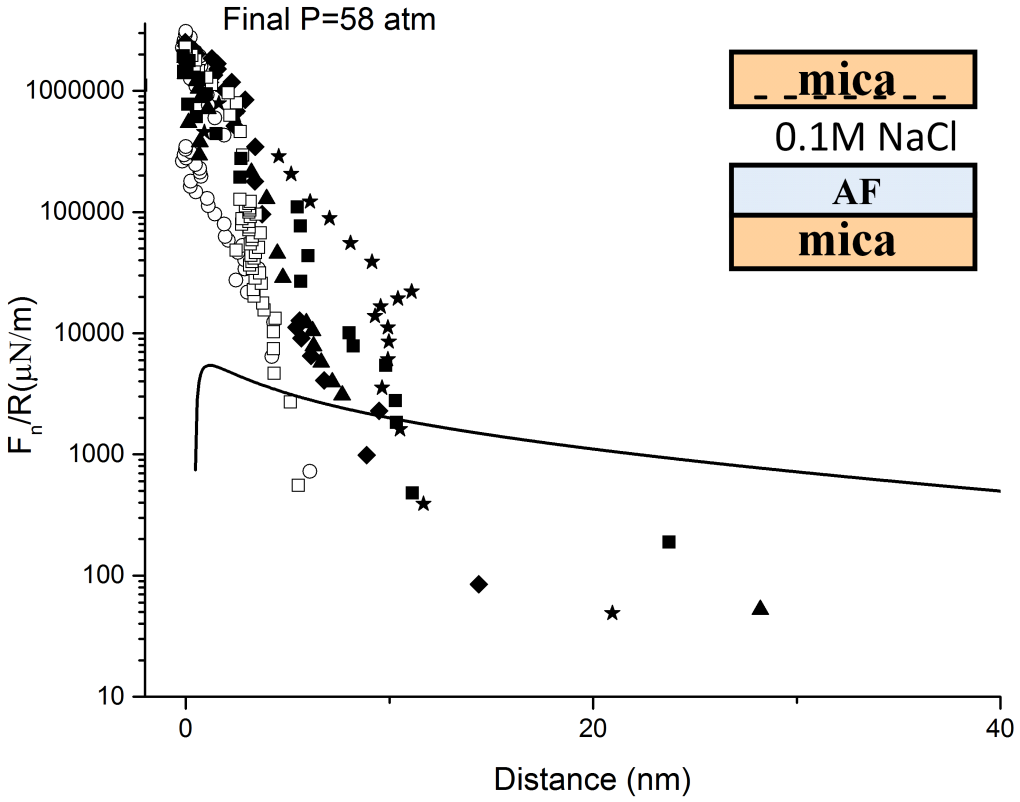

Figure 2: Force profiles between AF and mica surfaces. (A) Profiles of normalized force $F_n(D)/R$ vs. separation D profiles across pure water between bare mica and the surface of an AF layer spin-cast on mica (left inset cartoon); monotonic repulsion above the scatter commenced from D = ca. 150 nm. Filled, empty and half-empty symbols refer to profiles measured on approach, on separation and a second approach at a given point respectively. Blue curve: Calculated $F_n(D)/R$ profile (based on (PB + vdW), Methods for details) for a negatively-charged mica (with characteristic $\sigma^{mica} = -e/(66.5nm^2)$,[30]) facing an uncharged AF surface ($\sigma^{AF} = 0$). The much lower calculated repulsion (blue curve) compared to the measured repulsion (red data) reveals that the AF surface is also negatively charged. Black curve: calculated $F_n(D)/R$ profile using same parameters as for blue curve but with $\sigma^{AF} = -e/(9\ nm^2)$, as indicated by other studies (SI section 4). The right inset shows schematically the SFB configuration, with K_n and K_s the normal and shear springs respectively, and P the sectored piezoelectric

tube enabling both normal and lateral motion (Methods). (B) $F_n(D)/R$ profiles across 0.1M NaCl solution between bare mica and an AF layer spin-cast on mica (cartoon). Filled and empty symbols refer to profiles measured on approach and on separation respectively. The black curve is the fit to the pure water data shown as the black curve in (A). The scatter in the data arises due to factors discussed in the text. We note that within a given profile at a given contact point, the scatter is much lower, *e.g.* red solid squares, hexagons or half-filled stars.

A

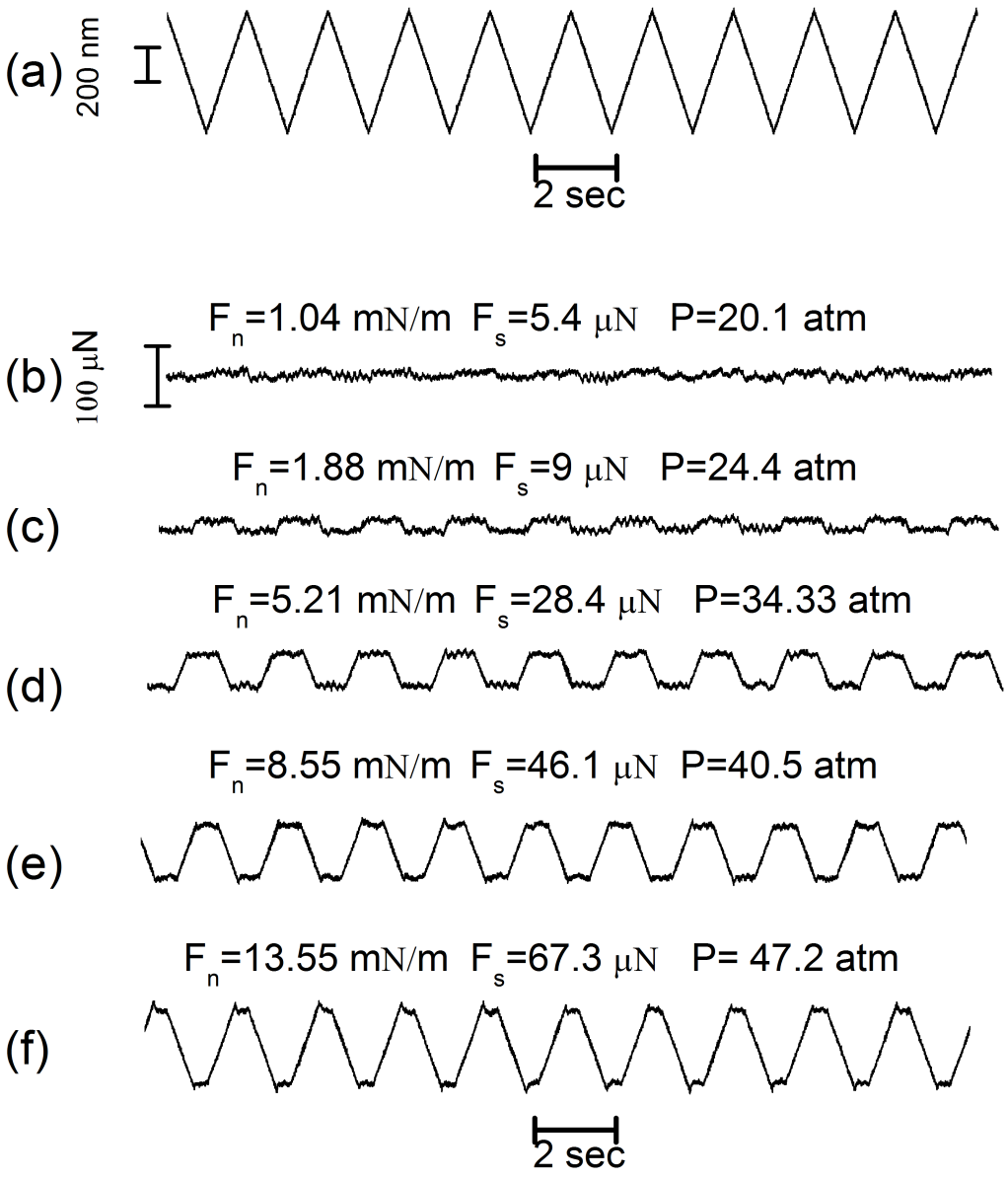
(a)
200 nm
2 sec
F_n=1.04 mN/m F_s=5.4 μN P=20.1 atm
(b)
100 μN
F_n=1.88 mN/m F_s=9 μN P=24.4 atm
(c)
F_n=5.21 mN/m F_s=28.4 μN P=34.33 atm
(d)
F_n=8.55 mN/m F_s=46.1 μN P=40.5 atm
(e)
F_n=13.55 mN/m F_s=67.3 μN P= 47.2 atm
(f)
2 sec

B

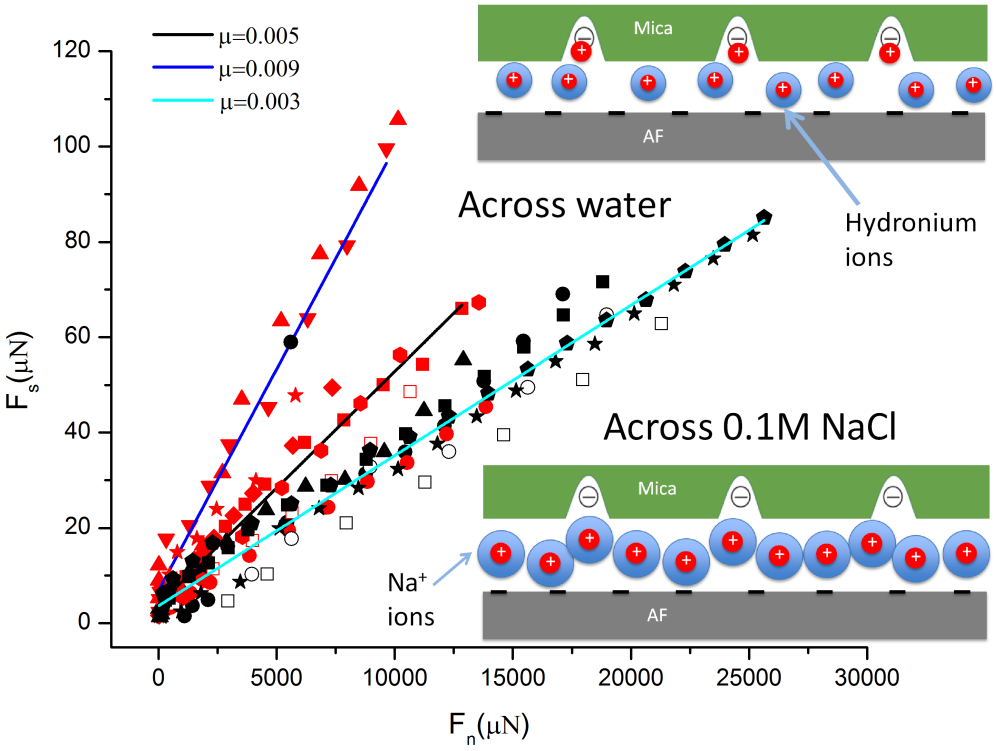

Figure 3: Sliding friction between AF and mica surfaces. (A) Typical shear force (F_s) *versus* time traces for water-immersed surfaces. Trace (a) shows the applied back and forth lateral motion Δx_0 of the upper (bare mica) surface sliding past the lower AF-coated mica surface at increasing loads F_n (and corresponding pressures P), at a typical mid-range sliding velocity (v_s = 730 nm/sec). Traces (b - f) show the corresponding shear traces, taken directly from the bending of the shear spring K_s (fig. 2A inset). The average friction force, F_s was evaluated from the sliding plateau region of the traces (and where the signal is weak, as in traces (b) and (c), was evaluated *via* a fast Fourier transform algorithm at the drive frequency (SI section 3)). (B) Summary of the measured friction forces F_s as a function of applied loads F_n taken from traces as in (A). Red symbols: measured in water. Black symbols: measured in 0.1M NaCl. Full and empty symbols: measured during approach and

separation profiles respectively (data shown are all for the same mid-range sliding velocity v_s = 730 nm/sec; the (weak) variation of F_s with v_s is shown in fig. 4). The inset cartoons illustrate the proposed interfacial configurations under strong compression in water (upper) and 0.1M NaCl (lower), indicating the hydrated (positively-charged) hydronium and Na^+ counterions, respectively, trapped between the negatively-charged surfaces (and the neutralized and charged mica surface lattices in the case of water and salt respectively, see text). Results in (B) are based on shear traces (as in (A)) taken over a total of 12 different approach (and in several cases also separation) profiles from 4 independent experiments.

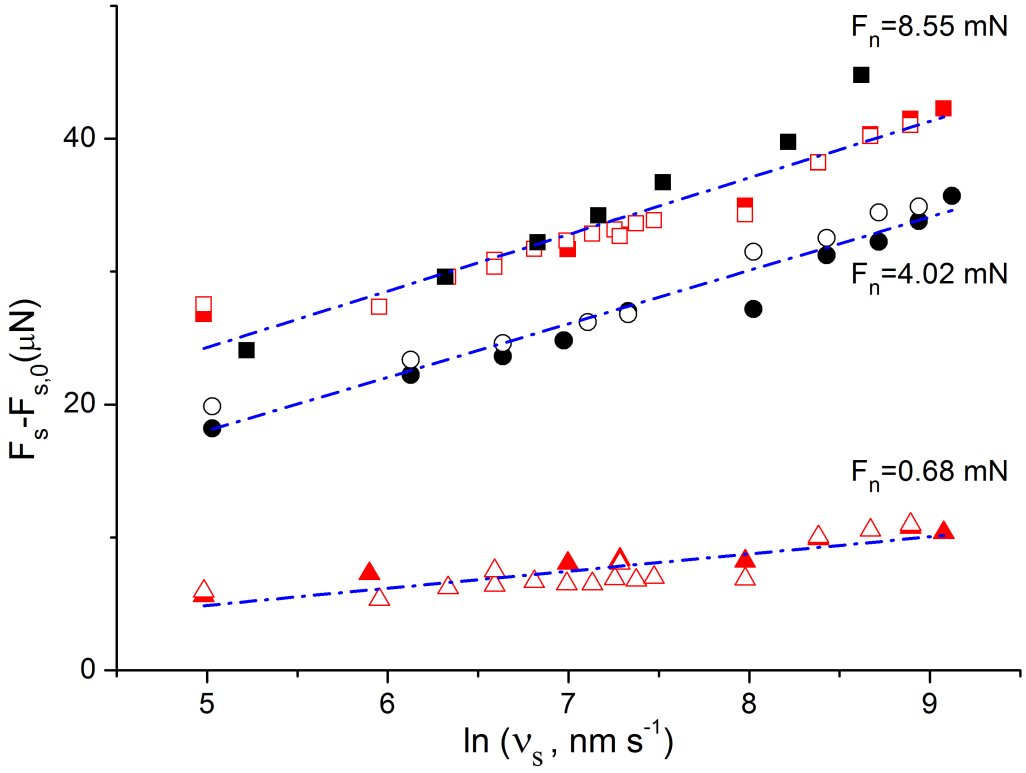

Figure 4: Variation of shear force with the sliding velocity v_s between bare mica and AF surfaces at different loads F_n. The data are plotted as (F_s - $F_{s,0}$) *versus* ln(v_s), where $F_{s,0}$ is a small systematic background signal unrelated to the shear force between the surfaces, and is determined separately for each contact point and velocity (Methods).

Red symbols: measured across water; black symbols: measured across 0.1M NaCl solution. Full and empty symbols were measured while increasing or reducing the velocity respectively. Broken lines at each load are best linear fit, $(F_s - F_{s,0}) = (\text{constant}) + (\text{constant})\ln(\underline{v}_s)$ indicating a rate activated process (Methods).

References

1. Lee, S.; Spencer, N. D., Aqueous Lubrication of Polymers: Influence of Surface Modification. *Tribol. Int.* **2005**, 38, 922-930.

2. Andersson, H.; van der Wijngaart, W.; Griss, P.; Niklaus, F.; Stemme, G., Hydrophobic Valves of Plasma Deposited Octafluorocyclobutane in DRIE Channels. *Sens. Actuators, B* **2001**, 75, 136-141.

3. Choo, J. H.; Spikes, H. A.; Ratoi, M.; Glovnea, R.; Forrest, A., Friction Reduction in Low-Load Hydrodynamic Lubrication with a Hydrophobic Surface. *Tribol. Int.* **2007**, 40, 154-159.

4. Hiratsuka, K.; Bohno, A.; Endo, H., Water Droplet Lubrication Between Hydrophilic and Hydrophobic Surfaces. *J. Phys.: Conf. Ser.* **2007**, 89, 012012.

5. Hansson, P. M.; Claesson, P. M.; Swerin, A.; Briscoe, W. H.; Schoelkopf, J.; Gane, P. A. C.; Thormann, E., Frictional Forces Between Hydrophilic and Hydrophobic Particle Coated Nanostructured Surfaces. *Phys. Chem. Chem. Phys.* **2013**, 15, 17893-17902.

6. Khademhosseini, A.; Langer, R.; Borenstein, J.; Vacanti, J. P., Microscale Technologies for Tissue Engineering and Biology. *Proc. Natl. Acad. Sci. U. S. A.* **2006**, 103, 2480-2487.

7. Krafft, M. P., Fluorocarbons and Fluorinated Amphiphiles in Drug Delivery and Biomedical Research. *Adv. Drug Delivery Rev.* **2001**, 47, 209-228.

8. Suk, J. W.; Cho, J. H., Capillary Flow Control Using Hydrophobic Patterns. *J. Micromech. Microeng.* **2007**, 17, N11-N15.

9. Williams, D. F., On the Mechanisms of Biocompatibility. *Biomaterials* **2008**, 29, 2941-2953.

10. Rojas, O. J.; Macakova, L.; Blomberg, E.; Emmer, A.; Claesson, P. M., Fluorosurfactant Self-Assembly at Solid/Liquid Interfaces. *Langmuir* **2002**, 18, 8085-8095.

11. Christenson, H. K.; Claesson, P. M., Direct Measurements of the Forces Between Hydrophobic Surfaces in Water. *Adv. Colloid Interface Sci.* **2001**, 91, 391-436.

12. Binks, B. P.; Clint, J. H., Solid Wettability from Surface Energy Components: Relevance to Pickering Emulsions. *Langmuir* **2002**, 18, 1270-1273.

13. Chandler, D., Interfaces and the Driving Force of Hydrophobic Assembly. *Nature* **2005**, 437, 640-647.

14. FreijLarsson, C.; Nylander, T.; Jannasch, P.; Wesslen, B., Adsorption Behaviour of Amphiphilic Polymers at Hydrophobic Surfaces: Effects on Protein Adsorption. *Biomaterials* **1996**, 17, 2199-2207.

15. Jensen, T. R.; Jensen, M. O.; Reitzel, N.; Balashev, K.; Peters, G. H.; Kjaer, K.; Bjornholm, T., Water in Contact with Extended Hydrophobic Surfaces: Direct Evidence of Weak Dewetting. *Phys. Rev. Lett.* **2003**, 90, 086101.

16. Lee, R. G.; Kim, S. W., Adsorption of Proteins onto Hydrophobic Polymer Surfaces - Adsorption-Isotherms and Kinetics. *J. Biomed. Mater. Res.* **1974**, 8, 251-259.

17. Meyer, E. E.; Rosenberg, K. J.; Israelachvili, J., Recent Progress in Understanding Hydrophobic Interactions. *Proc. Natl. Acad. Sci. U. S. A* **2006**, 103, 15739-15746.

18. Pal, S.; Roccatano, D.; Weiss, H.; Keller, H.; Muller-Plathe, F., Molecular Dynamics Simulation of Water near Nanostructured Hydrophobic Surfaces: Interfacial Energies. *ChemPhysChem* **2005**, 6, 1641-1649.

19. Samson, J. S.; Scheu, R.; Smolentsev, N.; Rick, S. W.; Roke, S., Sum Frequency Spectroscopy of the Hydrophobic Nanodroplet/Water Interface: Absence of Hydroxyl Ion and Dangling Oh Bond Signatures. *Chem. Phys. Lett.* **2014**, 615, 124-131.

20. Sigal, G. B.; Mrksich, M.; Whitesides, G. M., Effect of Surface Wettability on the Adsorption of Proteins and Detergents. *J. Am. Chem. Soc.* **1998**, 120, 3464-3473.

21. Tanford, C., Interfacial Free-Energy and the Hydrophobic Effect. *Proc. Natl. Acad. Sci. U. S. A.* **1979**, 76, 4175-4176.

22. Bowden, F. P.; Tabor, D., The Friction and Lubrication of Solids. *Oxford*, **2001**; Vol. Oxford University Press.

23. Tabor, D., Friction as a Dissipative Process. In Fundamentals of Friction: Macroscopic and Microscopic Processes, Singer, I. L. and Pollock, H. M. Eds., *Kluwer Academic Publishers*, Dortrecht, **1992**, pp. 3-24.

24. Donaldson, S. H.; Das, S.; Gebbie, M. A.; Rapp, M.; Jones, L. C.; Roiter, Y.; Koenig, P. H.; Gizaw, Y.; Israelachvili, J. N., Asymmetric Electrostatic and Hydrophobic-Hydrophilic Interaction Forces Between Mica Surfaces and Silicone Polymer Thin Films. *ACS Nano* **2013**, 7, 10094-10104.

25. Drechslera, A.; N. Petonga, N.; Zhangb, J.; Kwokb, D. Y.; Grundkea, K., Force Measurements Between Teflon Af and Colloidal Silica Particles in Electrolyte Solutions. *Colloids Surf., A* **2004**, 250, 357–366.

26. Ducker, W. A.; Xu, Z. G.; Israelachvili, J. N., Measurements of Hydrophobic and DLVO Forces in Bubble-Surface Interactions in Aqueous-Solutions. *Langmuir* **1994**, 10, 3279-3289.

27. Kaggwa, G. B.; Nalam, P. C.; Kilpatrick, J. I.; Spencer, N. D.; Jarvis, S. P., Impact of Hydrophilic/Hydrophobic Surface Chemistry on Hydration Forces in the Absence of Confinement. *Langmuir* **2012**, 28, 6589-6594.

28. Kokkoli, E.; Zukoski, C. F., Surface Forces Between Hydrophilic Self-Assembled Monolayers in Aqueous Electrolytes. *Langmuir* **2000**, 16, 6029-6036.

29. Meagher, L.; Pashley, R. M., Interaction Forces Between Silica and Polypropylene Surfaces in Aqueous-Solution. *Langmuir* **1995**, 11, 4019-4024.

30. Parker, J. L.; Claesson, P. M., Forces Between Hydrophobic Silanated Glass Surfaces. *Langmuir* **1994**, 10, 635-639.

31. Faghihnejad, A.; Zeng, H., Interaction Mechanism Between Hydrophobic and Hydrophilic Surfaces: Using Polystyrene and Mica as a Model System. *Langmuir* **2013**, 29, 12443-12451.

32. Hozumi, A.; Sugimura, H.; Yokogawa, Y.; Kameyama, T.; Takai, O., Zeta-Potentials of Planar Silicon Plates Covered with Alkyl- and Fluoroalkylsilane Self-Assembled Monolayers. *Colloids Surf., A* **2001**, 182, 257-261.

33. Preocanin, T.; Selmani, A.; Lindqvist-Reis, P.; Heberling, F.; Kallay, N.; Lutzenkirchen, J., Surface Charge at Teflon/Aqueous Solution of Potassium Chloride Interfaces. *Colloids Surf., A* **2012**, 412, 120-128.

34. Welzel, P. B.; Rauwolf, C.; Yudin, O.; Grundke, K., Influence of Aqueous Electrolytes on the Wetting Behavior of Hydrophobic Solid Polymers - Low-Rate Dynamic Liquid/Fluid Contact Angle Measurements Using Axisymmetric Drop Shape Analysis. *J. Colloid Interface Sci.* **2002**, 251, 101-108.

35. Zimmermann, R.; Dukhin, S.; Werner, C., Electrokinetic Measurements Reveal Interfacial Charge at Polymer Films Caused by Simple Electrolyte Ions. *J. Phys. Chem. B* **2001**, 105, 8544-8549.

36. Theander, K.; Pugh, R. J.; Rutland, M. W., Forces and Friction Between Hydrophilic and Hydrophobic Surfaces: Influence of Oleate Species. *J. Colloid Interface Sci.* **2007**, 313, 735-746.

37. Clear, S. C.; Nealey, P. F., Chemical Force Microscopy Study of Adhesion and Friction Between Surfaces Functionalized with Self-Assembled Monolayers and Immersed in Solvents. *J. Colloid Interface Sci.***1999**, 213, 238-250.

38. Klein, J.; Kumacheva, E., Simple Liquids Confined to Molecularly Thin Layers. I. Confinement-Induced Liquid to Solid Phase Transitions. *J. Chem. Phys.* **1998**, 108, 6996-7009.

39. Israelachvili, J. N., Intermolecular and Surface Forces. 2nd ed.; Academic Press Limited: *London*, **1992**.

40. Pashley, R. M., Hydration Forces Between Mica Surfaces in Aqueous Electrolyte Solutions. *J. Colloid Interface Sci.* **1981**, 80, 153-162.

41. Raviv, U.; Laurat, P.; Klein, J., Time - Dependence of Forces Between Mica Surfaces in Water and Its Relation to the Release of Surface Ions. *J. Chem. Phys.* **2002**, 116, 5167-5172.

42. Beattie, J. K.; Djerdjev, A. M., The Pristine Oil/Water Interface: Surfactant-Free Hydroxide-Charged Emulsions. Angew. *Chem., Int. Ed.* **2004**, 43, 3568-3571.

43. Raviv, U.; Klein, J., Fluidity of Bound Hydration Layers. *Science* **2002**, 297, 1540-1543.

44. Gaisinskaya-Kipnis, A.; Ma, L.; Kampf, N.; Klein, J., Frictional Dissipation Pathways Mediated by Hydrated Alkali Metal Ions. *Langmuir* **2016**, 32, 4755-4764.

45. Ma, L.; Gaisinskaya, A.; Kampf, N.; Klein, J., Origins of Hydration Lubrication. *Nature Comm.* **2015**, 6, 6060.

46. Biswas, S. K.; Vijayan, K., Friction and Wear of PTFE — a Review. *Wear* **1992**, 158, 193-211.

47. Sorkin, R.; Kampf, N.; Dror, Y.; Shimoni, E.; Klein, J., Origins of Extreme Boundary Lubrication by Phosphatidylcholine Liposomes. *Biomaterials* **2013**, 34, 5465-5475.

48. Tivony, R., Interactions Between Dissimilar Surfaces in Aqueous Media at Controlled Potentials. Ph.D. thesis, Weizmann Institute of Science, Israel, **2017**.

49. Tyrrell, J. W. G.; Attard, P., Images of Nanobubbles on Hydrophobic Surfaces and Their Interactions. *Phys. Rev. Lett.* **2001**, 87, 176104.

50. Zhang, X. H.; Maeda, N.; Craig, V. S. J., Physical Properties of Nanobubbles on Hydrophobic Surfaces in Water and Aqueous Solutions. *Langmuir* **2006**, 22, 5025-5035.

51. Christenson, H. K.; Claesson, P. M., Cavitation and the Interaction Between Macroscopic Hydrophobic Surfaces. *Science* **1988**, 239, 390-392.

52. Raviv, U.; Laurat, P.; Klein, J., Fluidity of Water Confined to Sub-Nanometre Films. *Nature* **2001**, 413, 51-54.

53. Kanduč, M.; Netz, R. R., From Hydration Repulsion to Dry Adhesion Between Asymmetric Hydrophilic and Hydrophobic Surfaces. *Proc. Natl. Acad. Sci. U. S. A.* **2015**, 112, 12338-12343.

54. Maduar, S. R.; Belyaev, A. V.; Lobaskin, V.; Vinogradova, O. I., Electrohydrodynamics near Hydrophobic Surfaces. *Phys. Rev. Lett.* **2015**, 114, 118301.

55. Cottin-Bizonne, C.; Cross, B.; Steinberger, A.; Charlaix, E., Boundary Slip on Smooth Hdrophobic Surfaces: Intrinsic Effects and Possible Artifacts. *Phy. Rev. Lett.* **2005**, 94, 056102.

56. Zhan, C.-G.; Dixon, D. A., Absolute Hydration Free Energy of the Proton from First-Principles Electronic Structure Calculations. *J. Phys. Chem. A* **2001**, 105, 11534-11540.

57. Perkin, S.; Chai, L.; Kampf, N.; Raviv, U.; Briscoe, W. H.; Dunlop, I. E.; Titmuss, S.; Seo, M.; Kumacheva, E.; Klein, J., Forces Between Mica Surfaces, Prepared in Different Ways, Across Aqueous and Non-Aqueous Liquids Confined to Molecularly Thin Films. *Langmuir* **2006**, 22, 6142-6152.

58. Nightingale, E. R., Phenomenological Theory of Ion Solvation. Effective Radii of Hydration Ions. *J. Phys. Chem.* **1959**, 63, 1381-1387.

59. Espinosa-Marzal, R. M.; Drobek, T.; Balmer, T.; Heuberger, M., Hydrated Ion Ordering in Electrical Double Layers. *Phys. Chem. Chem. Phys.* **2012**, 14, 6085-6093.

60. Briscoe, B. J.; Evans, D. C. B., The Shear Properties of Langmuir-Blodgett Layers. *Proc. R. Soc. London, Ser. A* **1982**, 380, 389-407.

61. Ben-Yaakov, D.; Andelman, D., Revisiting the Poisson-Boltzmann Theory: Charge Surfaces, Multivalent Ions and Inter-Plate Forces. *Phys. A (Amsterdam, Neth.)* **2010**, 389, 2956-2961.

62. Drummond, C. J.; Georgaklis, G.; Chan, D. Y. C., Fluorocarbons: Surface Free Energies and Van Der Waals Interaction. *Langmuir* **1996**, 12, 2617-2621.

63. Kampf, N.; Ben-Yaakov, D.; Andelman, D.; Safran, S. A.; Klein, J., Direct Measurement of Sub-Debye-Length Attraction Between Oppositely Charged Surfaces. *Phys. Rev. Lett.* **2009**, 103, 118304-1 - 118304-4.

Supplementary Information for:

Trapped Aqueous Films Lubricate Highly-Hydrophobic Surfaces.

Irit Rosenhek-Goldian‡, Nir Kampf‡, and Jacob Klein*

Dept. of Materials and Interfaces, Weizmann Institute of Science, Rehovot 76100, Israel

‡ These authors contributed equally

* Jacob.klein@weizmann.ac.il

Contents:

1. Molecular structure of fluoropolymer and solvent
2. Surface force balance (SFB)
3. Experimental procedure, and shear and normal force measurement
4. Estimate of surface charge density on AF surface
5. Concerning the nature of the charge on AF in water
6. Concerning friction between two hydrophobic surfaces under water

1. Molecular structure of fluoropolymer and solvent:

The molecular structure of the amorphous fluoropolymer, Poly[4,5-difluoro-2,2-bis(trifluoromethyl)-l,3- dioxole-co-tetrafluoroethylene] , (DuPont™ Teflon® AF 1600 (AF)). (m:n=1:2) is given in fig. 1a[1].

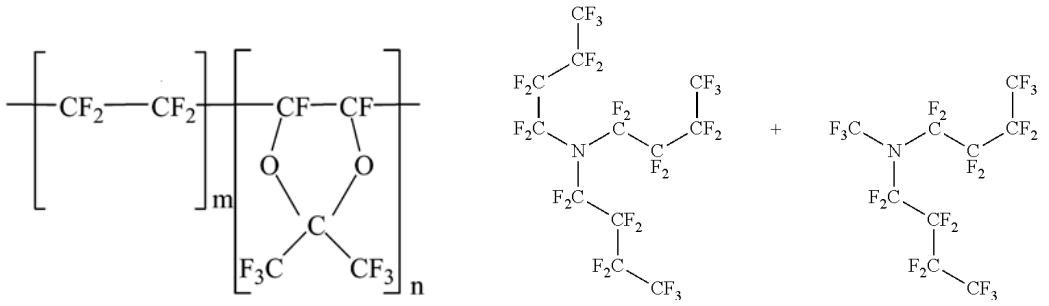

a b

The molecular structure of the solvent used for the AF1600 is shown in fig. 1b; perfluoro-tributyl amine solvent 3M Fluorinert® FC-40, which is a mixture of perfluorinated amine $N(C_4F_9)_3$ and $CF_3N(C_4F_9)_2$ having average MW of 650.[2]

2. Surface force balance (SFB)

The SFB used in our experiment was similar to that described by Klein and Kumacheva[3], and is shown schematically in the inset to Fig. 2A of the main text. Its principle features are, briefly, as follows. Single crystal mica sheets (thickness ca. 2-3 μm) are cleaved (as described in ref.[4] to avoid contamination), back-silvered and mounted on crossed cylindrical lenses within the SFB, and their relative normal separation and lateral motion is controlled *via* a 3-stage system, the most sensitive of which is the sectored piezoelectric tube P (inset to fig. 2A). White-light multiple beam interferometry enables measurement of the surface separation, *D* (at the point of closest approach), between the mica surfaces (optimally to ±0.2 - 0.3 nm), and allows the

geometry of the contact area (including the mean radius of curvature of the mica surfaces $R \approx 1$ cm) and any flattening of the surfaces, under load or adhesion, to be determined. The bending of the normal force and shear force springs (K_n and K_s in the inset to fig. 2A, of known spring constants) are determined through the interferometric measurements of D and changes in air-gap capacitance (to ±0.3 nm), respectively, and this bending yields the normal and shear forces directly.

3. Experimental procedure:

Cleaning procedure: Before every experiment, glassware was cleaned by immersion for an hour in a fresh mixture of hydrogen peroxide H_2O_2 (30% solution) and sulfuric acid H_2SO_4 (95 - 97 %, solution) in volume ratio of 3:7. The glassware was rinsed with deionized and conductivity water, sonicated in conductivity water and then ethanol, rinsed with filtered ethanol and finally dried in a laminar flow cabinet. All metal tools and attachments of the SFB in direct contact with the surfaces and solution were immersed for an hour in a hot (80°C) 1:1mixture of conductivity water and nitric acid HNO_3 (66 %, solution). The metal tools were then sonicated for ca. 10 min in conductivity water and then with ethanol, rinsed with filtered ethanol and finally dried in a laminar flow cabinet.

Normal forces measurement: The lower mica surface is mounted on a horizontal leaf spring (spring constant K_n = 150 N/m) whose bending ΔD is measured by interferometry to yield the normal forces F_n(D) with sensitivity ca. ±50nN in optimal conditions.

Shear forces measurement: Friction measurement by the SFB involves the application of parallel lateral motion between the surfaces *via* the sectored piezo-tube holding the upper mica sheet, as has been described in detail previously[3]. Shear motion is applied by ramping the

potential (triangular waveform) on a sectored piezo tube, leading to an overall back and forth lateral motion, Δx_0, of the upper surface. Shear forces, $F_s(D) = K_s.\Delta x(t)$, transmitted between the surfaces are monitored *via* the bending $\Delta x(t)$ of the shear springs (spring constant $K_s = 300$ N/m), determined to ca. ±0.3 nm using the air gap capacitor (Accumeasure ASP-1-ILA, MTI Instruments, NY). The output is a time trace of the shear spring bending, examples of which are shown in fig. 3A (main text).

In order to minimize ambient vibrations, an electronic vibration isolation system (Halcyonics, MOD-1L, Gottingen, Germany) is used. The noise level in these experiments was higher than reported in some earlier experiments, corresponding to noise in the shear force of ca. ±0.5 – 1.0 μN, before signal processing. To improve signal to noise, the shear traces were frequency-analyzed (fast Fourier transformed, FFT) and the amplitude of signal at the applied frequency was determined both with the surfaces far apart and at progressively smaller separations. A small systematic error, arising from a weak coupling of the shear springs of the SFB to the body of the apparatus *via* the thin PZT connection wires, results in a small signal $F_{s,0}$ (at the drive frequency[5]), which is not related to the shear force between the surfaces and which depends on the amplitude Δx_0 of lateral motion applied to the top surface[3]. It is evaluated from measurements at large D where the shear force between the surfaces vanishes, and may be subtracted (as in fig. 6) from the value of F_s (we emphasize that in general $F_s >> F_{s,0}$).

4. Estimate of surface charge density on AF surface

The measured surface charge density at the water/(hydrophobic) hexadecane interface determined in the study of ref.[6] at pH ≈ 8 is $\sigma \approx -e/(3\text{nm}^2)$, and we take the surface charge density at the water/(hydrophobic) AF interface at such a pH (= 8) value to be similar. The corresponding surface potential ψ_0 at the AF surface, using the Grahame equation[7]

$\sigma = \sqrt{8\varepsilon\varepsilon_0 k_B T}\,\sinh(\frac{e\psi_0}{2k_B T})\sqrt{c_\infty}$, (where e is the electronic charge, ε and ε_0 the dielectric constant and free-space-permeability constant respectively, k_B and T have their usual meaning, and c_∞ is the bulk salt concentration) is $\psi_0 \approx$ -240 mV (where c_∞ is taken equivalent to ca. $8\text{x}10^{-5}$ M 1:1 electrolyte for the no-added-salt water, see fig. 2). From ref.[8], the increase in the zeta potential of an AF surface on going from pH = 8 to pH = 6 is ca. 55 mV. If we make the reasonable assumption that this pH change results in a similar change also in the surface potential, this yields $\psi_0 \approx$ (-240 + 55) mV $\approx$ -185 mV. Inserting this value in the Grahame equation yields $\sigma^{AF} \approx -e/(9\ \text{nm}^2)$. This is the value used to generate, the Poisson-Boltzmann equation augmented by vdW interactions (Methods section in main text), the black curve through the data in fig. 2A of the main text.

5. Concerning the nature of the charge on AF in water

The main conclusion from the repulsive $F_n(D)/R$ profiles of fig. 2A is that the AF surface under water is negatively charged, though the force profiles cannot reveal the origin of the charge. The more general issue of the precise nature, distribution and indeed sign of the charge at the interface of water with hydrophobic media is a topic of considerable debate, whose detailed consideration is beyond the scope of this work. In particular, the charge at the water/*air* interface (which differs from the water/solid-hydrophobic-surface in the present study), has been investigated in much detail using a wide variety of approaches, ranging from macroscopic surface tension studies to sophisticated spectroscopic/microscopic methods as well as computational approaches (see for example refs.[9-17]). Most (though not all) of these studies indicate a net positive charge at the air (or vapour)/water interface, arising from an excess of hydronium ions. In contrast, for the case of water in contact with a condensed-phase-hydrophobic or *solid*-hydrophobic surfaces, as in the present study, most of the studies suggest a negatively-charged interface at the pH $\approx$ 6 of the present experiments. Thus the negative

charge on the hydrophobic AF surface under water consistent with the $F_n(D)/R$ profiles of fig. 2A main text (black curve) is in line with ζ-potential measurements on inert hydrophobic solids such as PTFE[18], polystyrene, poly(vinyl chloride)[8], C18-trimethoxysilane on silica[19] and C18-thiol on gold[20], and in particular on an AF surface[8,21]. It is also in line with several previous force-measurement studies, using both SFBs and scanning force microscopy methods, showing repulsion across water between a hydrophobic and a (negatively-charged) hydrophilic surface[22-26]. In many of these studies (for example refs.[6,8,21,27-30]) of the water/hydrophobic-condensed-phase interface, an excess of the negatively-charged hydroxyl $–OH^-$ ion at this interface has been suggested as the origin of the negative charge, though also other possibilities have been suggested[31]. In any case, the presence of hydroxyl ions at the AF/water interface is not proven by the present results, nor is it essential for understanding the friction reduction, as we do, in terms of lubrication provided largely by trapped hydrated counterions.

6. Concerning friction between two hydrophobic surfaces under water

The present study considers the friction between a hydrophilic (mica) surface sliding across a hydrophobic (AF) surface. For completeness we note qualitatively that the case of friction between *two* hydrophobic AF surfaces, which is not within the scope of our investigation, is very different to the hydrophilic-hydrophobic situation of our study. This is because on approach to contact of two hydrophobic (AF) surfaces, a water-vapour-filled cavity may spontaneously form between them prior to contact[32-38], eliminating the liquid-water/solid-hydrophobic interface. This cavity collapses as the two hydrophobic surfaces come into intimate van der Waals (vdW) adhesive contact, leaving no water or hydrated ions between them to provide lubrication. Subsequent sliding between them entails substantial energy dissipation as the vdW adhesion contact is sheared, with consequent high friction[39].

References

1. Resnick, P. R.; Warren, H. B. In Modern fluoropolymers; John Scheirs Ed.; John Wiley & Sons: Chichester, **1997**; pp 397-419.

2. Hasi, W.; Zhao, H.; Lin, D.; He, W.; Lü, Z. Characteristics of Perfluorinated Amine Media for Stimulated Brillouin Scattering in Hundreds of Picoseconds Pulse Compression at 532 nm. *Chin. Opt. Lett.* **2015**, 13, 061901-061901.

3. Klein, J.; Kumacheva, E. Simple Liquids Confined to Molecularly Thin Layers. I. Confinement-Induced Liquid to Solid Phase Transitions. *J. Chem. Phys.* **1998**, 108, 6996-7009.

4. Perkin, S.; Chai, L.; Kampf, N; Raviv, U.; Briscoe, W.; Dunlop, I.; Titmuss, S; Seo, M.; Kumacheva, E.; Klein, J. Forces Between Mica Surfaces, Prepared in Different Ways, Across Aqueous and Non-Aqueous Liquids Confined to Molecularly Thin Films. *Langmuir* **2006**, 22, 6142-6152.

5. Raviv, U.; Laurat, P.; Klein, J. Fluidity of Water Confined to Sub-Nanometre Films. *Nature* **2001**,413, 51-54.

6. Beattie, J. K.; Djerdjev, A. M. The Pristine Oil/Water Interface: Surfactant-Free Hydroxide-Charged Emulsions. *Angew. Chem., Int. Ed.* **2004**, 43, 3568-3571.

7. Grahame, D. C. The Electrical Double Layer and the Theory of Electrocapillarity. *Chem. Rev.* **1947**, 41, 441-501.

8. Welzel, P. B.; Rauwolf, C.; Yudin, O.; Grundke, K. Influence of Aqueous Electrolytes on the Wetting Behavior of Hydrophobic Solid Polymers - Low-Rate Dynamic Liquid/Fluid Contact Angle Measurements Using Axisymmetric Drop Shape Analysis. *J. Colloid Interface Sci.* **2002**, 251, 101-108.

9. Beattie, J. K.; Djerdjev, A. N.; Warr, G. G. The Surface of Neat Water Is Basic. *Faraday Discuss.* **2009**, 141, 31-39.

10. Buch, V.; Milet, A.; Vacha, R.; Jungwirth, P.; Devlin, J. P. Water Surface Is Acidic. *Proc. Natl. Acad. Sci. U. S. A.* **2007**, 104, 7342-7347.

11. Iyengar, S. S.; Day, T. J. F.; Voth, G. A. On the Amphiphilic Behavior of the Hydrated Proton: An Ab Initio Molecular Dynamics Study. *Int. J. Mass Spectrom.* **2005,** 241, 197-204.

12. Petersen, M. K.; Iyengar, S. S.; Day, T. J. F.; Voth, G. A. The Hydrated Proton at the Water Liquid/Vapor Interface. *J. Phys. Chem. B* **2004,** 108, 14804-14806.

13. Petersen, P. B.; Saykally, R. J. Evidence for an Enhanced Hydronium Concentration at the Liquid Water Surface. *J. Phys. Chem. B* **2005** 109, 7976-7980.

14. Tarbuck, T. L.; Ota, S. T.; Richmond, G. L. Spectroscopic Studies of Solvated Hydrogen and Hydroxide Ions at Aqueous Surfaces. *J. Am. Chem. Soc.* **2006**, 128, 14519-14527.

15. Winter, B.; Faubel, M.; Vacha, R.; Jungwirth, P. Behavior of Hydroxide at the Water/Vapor Interface. *Chem. Phys. Lett.* **2009,** 474, 241-247.

16. Jungwirth, P. Spiers Memorial Lecture Ions at Aqueous Interfaces. *Faraday Discuss.* **2009,** 141, 9-30.

17. Wick, C. D.; Dang, L. X. J. The Behavior of NaOH at the Air-Water Interface: A *Computational Study. Chem. Phys.* **2010,** 133, 024705.

18. Preocanin, T.; Selmani, A.; Lindqvist-Reis, P.; Heberling, F.; Kallay, N.; Lützenkirchen, J. Surface Charge at Teflon/Aqueous Solution of Potassium Chloride Interfaces. *Colloids Surf., A* **2012,** 412, 120-128.

19. Hozumi, A.; Sugimura, H.; Yokogawa, Y.; Kameyama, T.; Takai, O. Zeta-Potentials of Planar Silicon Plates Covered with Alkyl- and Fluoroalkylsilane Self-Assembled Monolayers. *Colloids Surf., A* **2001**, 182, 257-261.

20. Schweiss, R.; Welzel, P. B.; Werner, C.; Knoll, W. Dissociation of Surface Functional Groups and Preferential Adsorption of Ions on Self-Assembled Monolayers Assessed by Streaming Potential and Streaming Current Measurements. Langmuir **2001,** 17, 4304-4311.

21. Zimmermann, R., Dukhin, S.; Werner, C. Electrokinetic Measurements Reveal Interfacial Charge at Polymer Films Caused by Simple Electrolyte Ions. *J. Phys. Chem. B* **2001,** 105, 8544-8549.

22. Donaldson, S. H.; Das, S.; Gebbie, M. A.; Rapp, M.; Jones, L. C.; Roiter, Y.; Koenig, P. H.; Gizaw, Y.; Israelachvili, J. N. Asymmetric Electrostatic and Hydrophobic-Hydrophilic Interaction Forces Between Mica Surfaces and Silicone Polymer Thin Films. *ACS Nano* **2013,** 7, 10094-10104.

23. Drechslera, A., N.; Petonga, N.; Zhangb, J.; Kwokb, D. Y.; Grundkea, K. Force Measurements Between Teflon AF and Colloidal Silica Particles in Electrolyte Solutions. *Colloids Surf., A* **2004,** 250, 357–366.

24. Kaggwa, G. B.; Nalam, P. C.; Kilpatrick, J. I.; Spencer, N. D.; Jarvis, S. P. Impact of Hydrophilic/Hydrophobic Surface Chemistry on Hydration Forces in the Absence of Confinement. *Langmuir* **2012,** 28, 6589-6594.

25. Meagher, L.; Pashley, R. M. Interaction Forces Between Silica and Polypropylene Surfaces in Aqueous-Solution. *Langmuir* **1995,** 11, 4019-4024.

26. Parker, J. L.; Claesson, P. M. Forces Between Hydrophobic Silanated Glass Surfaces. *Langmuir* **1994,** 10, 635-639.

27. Creux, P.; Lachaise, J.; Graciaa, A.; Beattie, J. K.; Djerdjev, A. M. Strong Specific Hydroxide Ion Binding at the Pristine Oil/Water and Air/Water Interfaces. *J. Phys. Chem. B* **2009,** 113, 14146-14150.

28. Marinova, K. G.; Alargova, R. G.; Denkov, N. D.; Velev, O. D.; Petsev, D. N.; Ivanov, I. B.; Borwankar, R. P. Charging of Oil-Water Interfaces Due to Spontaneous Adsorption of Hydroxyl Ions. *Langmuir* **1996,** 12, 2045-2051.

29. Kudin, K. N.; Car, R. Why Are Water-Hydrophobic Interfaces Charged? *J. Am. Chem. Soc.* **2008,**130, 3915-3919.

30. Tian, C. S.; Shen, Y. R. Structure and Charging of Hydrophobic Material/Water Interfaces Studied by Phase-Sensitive Sum-Frequency Vibrational Spectroscopy. Proc. *Natl. Acad. Sci. U. S. A.* **2009,** 106, 15148-15153.

31. Samson, J. S.; Scheu, R.; Smolentsev, N.; Rick, S. W.; Roke, S. Sum Frequency Spectroscopy of the Hydrophobic Nanodroplet/Water Interface: Absence of Hydroxyl Ion and Dangling OH Bond Signatures. *Chem. Phys. Lett.* **2014,** 615, 124-131.

32. Christenson, H. K.; Claesson, P. M. Cavitation and the Interaction Between Macroscopic Hydrophobic Surfaces. *Science* **1988,** 239, 390-392 ().

33. Christenson, H. K.; Claesson, P. M. Direct Measurements of the Forces Between Hydrophobic Surfaces in Water. *Adv. Colloid Interface Sci.* **2001,** 91, 391-436.

34. Ducker, W. A.; Xu, Z. G.; Israelachvili, J. N. Measurements of Hydrophobic and DLVO Forces in Bubble-Surface Interactions in Aqueous-Solutions. *Langmuir* **1994,** 10, 3279-3289.

35. Singh, S., Houston, J.; van Swol, F.; Brinker, C. J. Superhydrophobicity: Drying Transition of Confined Water. *Nature* **2006,** 442, 526-526. doi:http://www.nature.com/nature/journal/v442/n7102/suppinfo/442526a_S1.html.

36. Yaminsky, V. V.; Yushchenko, V. S.; Amelina, E. A.; Shchukin, E. D. Cavity Formation Due to a Contact Between Particles in a Nonwetting Liquid. *J. Colloid Interface Sci.* **1983,** 96, 301-306. doi:http://dx.doi.org/10.1016/0021-9797(83)90034-6.

37. Yushchenko, V. S.; Yaminsky, V. V.; Shchukin, E. D. Interaction Between Particles in a Nonwetting Liquid. *J. Colloid Interface Sci.* **1983,** 96, 307-314, doi:http://dx.doi.org/10.1016/0021-9797(83)90035-8.

38. Rosenhek-Goldian, I.; Kampf, N.; Klein, J. Interactions between Two Hydrophobic Surfaces: Experimental Indications for Cavitation Induced Attraction. In preparation.

39. Tabor, D. Friction as a Dissipative Process. In Fundamentals of Friction: Macroscopic and Microscopic Processes, Singer, I. L. and Pollock, H. M. Eds., *Kluwer Academic Publishers*, Dortrecht, **1992**, pp. 3-24.